ELECTRONIC SUPPLEMENTAL INFORMATION

Pathways to low-cost electrochemical energy storage: a comparison of aqueous and nonaqueous flow batteries

Robert M. Darling[a,b,*], Kevin G. Gallagher[a,c,**], Jeffrey A. Kowalski[a,d], Seungbum Ha[a,c], and Fikile R. Brushett[a,d]

[a] Joint Center for Energy Storage Research

[b] United Technologies Research Center, 411 Silver Lane, East Hartford, CT, USA 06108

[c] Chemical Sciences and Engineering Division, Argonne National Laboratory, 9700 S Cass Avenue, Lemont, IL, USA 60439

[d] Department of Chemical Engineering, Massachusetts Institute of Technology, 77 Massachusetts Avenue, Cambridge, MA USA 02139

*corresponding author e-mail: darlinrm@utrc.utc.com

**corresponding author e-mail: kevin.gallagher@anl.gov

The following supplemental text provides details on the assumptions used to create the performance and cost estimations in the main text.

Balance of Plant Costs

An energy storage system to support the electricity grid requires a power conditioning system, mainly an inverter and transformer, to connect the stack that produces DC power to a utility operator owned transformer. Power electronics are a significant cost component, with estimates in the range of \$200-500 kW^{-1} for energy storage devices at rated power levels of 1-5 MW.[1, 2] The DOE Sunshot Program has a goal of reducing this number to \$100 kW^{-1} for installed photovoltaic generating systems with low cost.[3] We use a power conditioning system cost of \$250 kW^{-1} for current costs and \$75-150 kW^{-1} for projections of high-volume future state costs.

In addition to the power conditioning system (PCS), control electronics will be required to monitor and regulate the health and state of charge of the battery. These controls will also regulate battery temperature and any other auxiliary systems that might be needed, such as pumps. Busbars, cell interconnects, and electrical wiring is required for all systems, with a higher burden for the many connections required for a Lithium-ion battery. Control electronics along with heating and cooling components are taken to cost \$60 kW^{-1} for flow batteries. Lithium-ion batteries are charged \$300 kW^{-1} due to the temperature sensitivity, large number of interconnects, and robust state-of-charge controls needed. In comparison, lead-acid technology is less sensitive to state-of-charge control and requires fewer interconnections between voltage units. The lead-acid estimate assumes \$100 kW^{-1}. These costs are assumed to decrease by half for the high volume forecasts. Flow batteries require pumps to move the reactant from the tank to the reactor. We use \$50 kW^{-1} for each reactant stream that requires pumping[2] with a 40% decrease for future state projections. We utilize Equation S1 to calculate the total balance-of-plant and installation costs:

$$c_{bop} = c_{pcs} + c_{controls} + N_{flow}c_{pumps} \qquad \text{Equation S1}$$

Additional Contribution to Price

Many additional cost contributions are added to the materials and balance-of-plant costs to reach the final price for the energy storage system. These additions include, but are not limited to, items such as direct labor for assembly, depreciation of manufacturing equipment, variable costs, general costs, sales, administration costs, and profit. We provide estimates to capture these contributions, but acknowledge each system would benefit from an in-depth assessment for specific contributions. The goal of this work is to examine trends that exist among the chemistries and battery architectures considered rather than the exact price value for a specific chemistry. We estimate the additional costs that make up the end price in some instances by comparing the total costs to the reported range of prices for commercial systems. Our estimates are limited to the costs of the major components leaving the factory, and do not include installation and site preparation charges.

Lead-acid battery manufacturing is in a relatively mature state compared to the other battery technologies considered.[4] However, the new electrode fabrication required for incorporating significant quantities of carbon in C-PbAcid will improve as volumes increase.[5] Additionally, the high-volume production markets for lead-acid are not currently for the large and massive cells that would be used for annual production of 10 GW h of grid storage. However, C-PbAcid does not require the same level of manufacturing complexity as that of Li-ion cells, which are moisture sensitive and composed of many thin layers.[6] The long-run additional contribution to price is taken to be \$200 kW^{-1} for C-PbAcid with current production values assumed to be a factor of six higher, in line with the reported 2014 price for total equipment. The long-run additional contribution to price value is lower than the ~\$400 kW^{-1} estimated by Lipman for a 0.5 GW h annual production, reported here in 2014 dollars.[7] The 20 times higher manufacturing volume considered in this work justifies the lower value. The Li-ion system is assumed to have a long-run add-on cost of \$300 kW^{-1} for large-scale energy installations[8] and current values near \$1100 kW^{-1}.[9] The near and long-term additional costs for the flow battery are taken to be \$1550 kW^{-1} and \$50-125 kW^{-1} for aqueous assemblies and \$1550 kW^{-1} to \$75-150 kW^{-1} for nonaqueous assemblies, which likely require more complex manufacturing. As discussed in the main text, the lower additional contributions to price value for flow batteries are expected due to their simpler assembly and are derived from examining manufacturing cost projections for proton exchange membrane (PEM) fuel cells.[10, 11] The capital depreciation and labor costs for pressing, slitting, assembling, sealing, and conditioning the PEM fuel cell reactor is \$1.1 kW^{-1} for 2.4 GW annual production volume.[10] Correcting these manufacturing costs for the ~5x more area required for a flow battery results in ~\$6 kW^{-1}. These capital depreciation and labor costs are then marked up to include contributions of general sales and administration, profit, warrantee and others as descirbed below giving the final future state range of \$50-125 kW^{-1} for aqueous flow batteries and \$75-150 kW^{-1} for nonaqueous.

The world-wide Li-ion battery market was ~28 GW h in 2011.[12] However, projections of future battery sales, excluding automotive and grid storage, are an order of magnitude higher by 2025 (e.g., 100 GW h for consumer electronics alone in 2025[12]). If market penetration for energy storage on the order of >1% is achieved for long-duration grid storage or full electric vehicles, market size will grow tremendously. The large manufacturing volume and competitive market places will drive down costs to the levels similar to a tier 1 automotive supplier. The time scale for future state values projected here should be considered greater than 10 years from the publication of this work and likely longer. The Li-ion projections were taken from a peer-

reviewed model of bottom-up battery performance and cost (BatPaC).[6, 8] The calculation approach therein scales the capital equipment, direct labor, production area, and thus overhead, to match the design and production volume of the battery considered. For the Gr/LFP battery, a production volume on par with current values, ~1 GWh, is calculated to have a required capital expenditure of $300 per kW·h·y. BatPaC projects this value decreases to $100 per kW·h·y for the 10-GWh scale considered in this analysis. The financial cost structure in BatPaC translates this capital investment to a value of c_{add} of $60 per kW·h for the examined future state. This value is significantly less than the $220 per kW·h estimated in the 2014 Gr/LFP case in Table 4, but in agreement with other forecasts made for future-state battery prices.[12-14]

A comparison between the additional contributions to price structure of a flow battery is made to Gr/LFP for the future state case in Figure S1. We follow the BatPaC model for the financial overhead structure. This approach results in smaller absolute values for items such as general, sales, administration (GSA) and research and development (R&D) for flow batteries as compared to Li-ion as a result of the lower capital depreciation and labor contributions. In contrast, the warranty charge is a fixed percentage of the total battery price. Using a multiplier approach for the financial structure is common; however, there are likely additional fixed values that are not captured here. Future work specifically addressing a flow battery manufacturing plant and additional contribution to price is warranted. These c_{add} values are highly uncertain, but are included in an attempt to 1) close the gap between material costs and the price charged by a system manufacturer and 2) demonstrate the dramatic lowering of costs that must occur to reach long-term goals. Competitive pressures, benefits from scale, and learning by doing will all be driving forces for projected cost reductions. Whether or not these values are reached depends on both the existence of a profitable energy storage market that utilizes the chemistry in question and the quality of the engineering estimates.

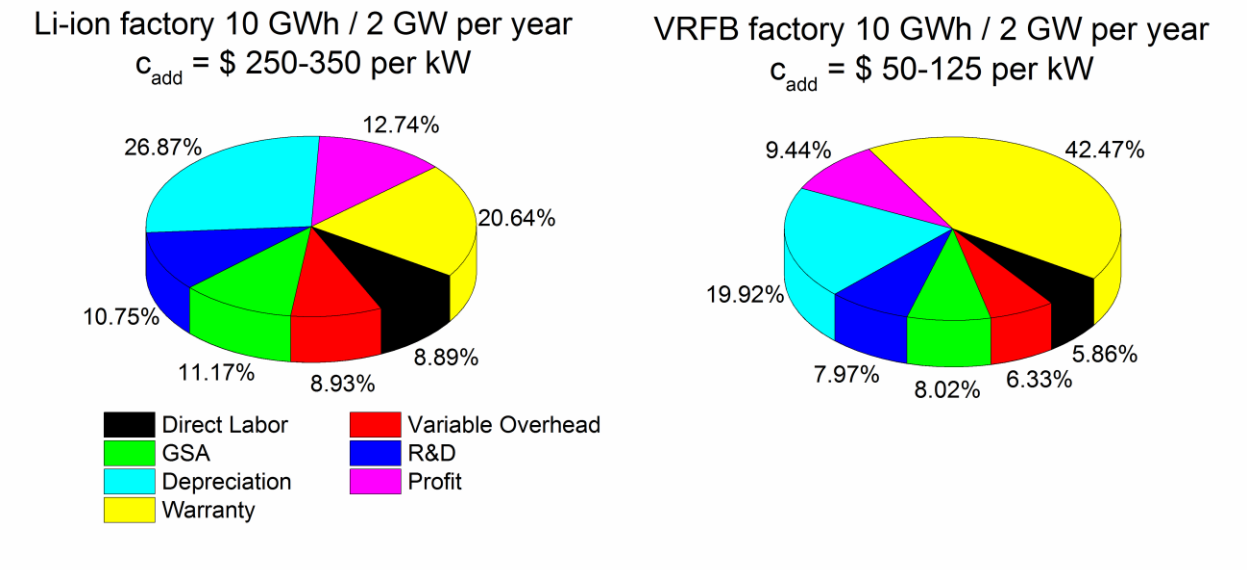

Figure S1. Comparison of financial structure of the additional contributions to price for a future state Gr/LFP Li-ion battery and a vanadium redox flow battery (VRFB).

Enclosed Architectures

Advanced Carbon Lead-Acid Batteries (C-PbAcid)

Various reports and papers were examined to determine a representative C-PbAcid battery design and cost for the energy storage applications considered.[1, 4, 7, 15-20] None of the existing reports provides the detail needed in this comparative analysis, and thus, engineering approximations were required based on the available information. The goal of our cost analysis is not to reproduce the exact advanced lead-acid technology used but to capture the primary physics and cost basis. A thick plate design is assumed for the advanced C-PbAcid technology due to the required 5-h characteristic discharge time. For this design, a 6-mm-thick positive plate is coupled with a 4-mm-thick negative plate, similar to traction batteries discussed in Linden and Reddy.[4]

The price of lead reported on the London Metal Exchange is \$2 kg^{-1} (http://www.lme.com/). PbO is the likely starting material in addition to minor paste components used for both the negative and positive plates, with the desired stoichiometry (i.e., PbO + PbO $\rightarrow$ Pb + PO_2) created during the formation process.[20] However, we normalize the active material cost to the properties of Pb and PbO_2. We use a baseline active mass price of \$3 kg^{-1} for the PbO_2 electrode. This assumes an additional cost above the pure lead price to account for processing lead into the active materials used in assembly. Some relatively new advanced C-PbAcid designs incorporate a significant quantity of carbon black into the negative electrode active mass to increase charge acceptance and cycle life. This is at times referred to as the Ultrabattery®.[19] Electrochemistry grade carbon black commonly costs around \$6-10 kg^{-1} and would add \$2 kg^{-1} to the price of lead active material assuming 20% by weight addition. We use \$5 kg^{-1} for negative electrode active material on a lead mass basis to reflect the use of carbon and other additives and binders in the assembly process. The manufacturing cost contributions for the pasting, drying, and curing of the active mass on the plates is captured in the additional contributions to price factor. The sulfuric acid electrolyte is a common commodity and inexpensive.[16]

The active mass utilization is a key parameter in determining the required quantity of lead used in the active materials, as C-PbAcid typically only uses a small fraction of the active mass.[17, 21] This utilization factor is in addition to the constrained SOC window traversed during operation. Following Srinivasan et al, we assume 27% utilization in the Pb negative electrode and 20% utilization in the PbO_2 positive electrode.[17] Utilization values as high as 50% have been reported but are common for high-power cells rather than the stationary, high-energy cells considered here.[20, 21] The area-specific resistance is estimated from performance reported in the literature for valve-regulated lead-acid.[17]

The required area is determined by the area capacity loading (mAh/cm^2) and the discharge time of the battery. We use 60 $mA \cdot h\ cm^{-2}$ for one half of the thickness of a 6 mm positive plate. The negative electrode is taken to have 1:1 balanced lead capacity to the positive assuming the additional carbon capacitance improves charge acceptance during the recharging process.[18, 19] The plates are taken to be lead or lead-alloy grids that have 90% void volume that will be filled by active material and sulfuric acid electrolyte. Area cost factors use one-half of each plate plus the addition of the separator. The grids are estimated to cost approximately \$16 m^{-2}, and the advanced glass matt separator is estimated to cost about \$4 m^{-2}. The grid costs are

derived from the cost of lead plus forming charge, while the separator matt is estimated from a range of costs for glass fibers, matt thickness of 1 mm, and porosity of 90%.[15]

Reported prices for advanced lead-acid systems span a wide range of values. Lead-acid traction batteries for electric vehicles or fork lifts are reported to cost $100-400 per kW·h at the pack level in 2014 dollars, excluding balance of plant.[7, 16] In comparison, installed grid storage applications with five hours of storage have reported total product costs of $350-1000 per kW·h, including balance of plant.[1] The differences in cost for the installed system generally reflect the allowable depth of discharge, with more expensive systems having a smaller operating window. Carbon lead-acid batteries have also been reported to cost $300-400 per kW·h in 2014 dollars.[19] Significant manufacturing cost reductions are expected if the volumes targeted within this study are reached.

Lithium-Ion Batteries

Lithium-ion batteries are in the process of entering new, high-volume markets after completely taking over the consumer electronics market during the last twenty years. Lithium-ion is quickly becoming the battery of choice for hybrid electric, plug-in hybrid, and full electric vehicle applications. In addition to transportation and consumer electronics applications that value energy density, the steep cost curve and high performance of Li-ion batteries are enabling their use in stationary applications. The price for an installed lithium-ion energy storage system for five hours of storage is reported to be $500-1000 per kW·h.[1, 9] We utilize the public domain BatPaC model to inform our performance values and long-run costs.[8] Estimates for current costs are derived from private communications. The negative electrode active material is a coated natural graphite and/or hard carbon material. The positive electrode assumed here is $LiFePO_4$. The electrolyte is commonly a mixture of linear carbonates, such as ethyl methyl carbonate (EMC) and ethylene carbonate (EC), with a $LiPF_6$ salt. The cost for the electrolyte follows the same assumption basis as other chemicals in this analysis. The cost per unit area in a Li-ion cell is low owing to the thin and relatively inexpensive nanoporous olefin separator, copper foils, and aluminum foil used. The main contributions to cost in a Li-ion battery are the active materials and electrolyte. However, current costs have a significant manufacturing overhead, which should be lowered as engineering advances are made on large-format cells and volumes increase.

Because of the low crystal density, required nanostructuring, and thus higher porosity in the $LiFePO_4$ (LFP) electrode, we limit the areal capacity to 2 mA·h cm^{-2}, which corresponds to 100 μm in thickness.[6] This loading assumption is supported by the teardown of a commercial Li-ion Gr/LFP cell as well as the BatPaC techno-economic model. Zheng et al. demonstrated this loading enables good performance and life for Gr/LFP.[22] Consumer electronics applications, such as cell phones and laptop computers, typically use high energy density lithium-ion cells based on layered oxides of $LiCoO_2$ or $LiNi_{0.8}Al_{0.15}Co_{0.05}O_2$ rather than LFP. These high energy density positive electrodes enable loadings of ~4-5 mAh/cm^2 of area capacity. However, the cells based on layered oxides are commonly less stable and of similar or greater cost as Gr/LFP chemistry. In grid storage applications, the size and weight of the battery (i.e., energy density) is not a significant selection driver. The improved stability and cycle life performance favor lower energy density chemistry like Gr/LFP. While the specific cost for area-based Li-ion components is low, the maximum electrode thickness limitation (i.e., 100 μm) results in much higher than desired electrode areas in the final design. We note that enclosed cells using aqueous electrolytes commonly achieve an order of magnitude higher thickness and, thus, area capacity loadings. Our lead-acid designs utilize 60 mA·h cm^{-2}.

A representative ASR for Li-ion batteries is 60 ohm-cm^2 for a constant discharge.[6, 8] The pulse power value is closer to 20 ohm-cm^2. The continuous discharge creates concentration gradients in the electrolyte and intercalation particles that manifest as a high resistance. Flow batteries typically overcome these gradients by utilizing convection to transport solubilized reactants.

Flow Electrode Architectures

Vanadium Redox Flow Batteries (VRFB)

Performance values are taken from in-house studies on a prototype short-stack VRFB. The cost of vanadium active material is taken from the historical average of vanadium prices available from the U.S. Geological Survey (USGS).[23] The price for vanadium metal was found to be similar to that given by V_2O_5 when normalized to the mass of the element. The vanadium prices show significant variation that is not well represented by a normal distribution generated from the standard deviation. A reasonable approach would be to represent the variation with a log-normal distribution. However, we chose to use a normal distribution to match the same statistical representation used with the other materials. The lower 95% confidence interval was set by the lowest reported annual value. The standard deviation was then taken to be one-half the difference between this value and the mean. The mean and 95% confidence interval plotted in Figure S2 capture the majority of the scatter, with two special cases with dramatic deviations to higher values. If a large VRFB market were established, a recycling stream for the vanadium could be created much like with lead-acid batteries. This closed life cycle would likely lead to a more predictable price for vanadium over time.

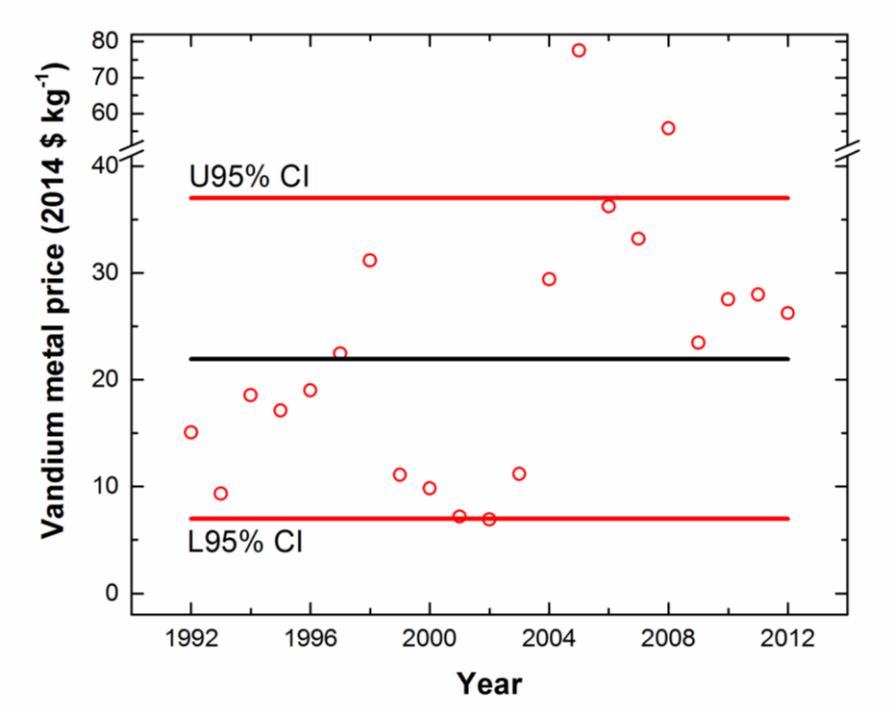

Figure S2. Vanadium metal price in 2014 US$ kg^{-1} from the USGS. The mean (black) and selected 95% confidence interval (red) are also shown.

Storage tanks suitable for sulfuric acid cost approximately $0.15 per L based on internet available pricing. This source of pricing does not reflect the lower values which will inevitably be obtained through a negotiation over high volume pricing. The aforementioned cost translates to $1.90 per kg of vanadium for an electrolyte containing 1.6 M vanadium. Storage costs will decrease with increasing concentration of active material, for the same materials of construction.

Aqueous Tailored Molecule Flow Batteries (AqRFB)

Tailored molecules are viable choices in aqueous and nonaqueous electrolytes. As of the time of this publication, a commercial tailored molecule system does not exist. However, many researchers are attempting to create new, promising charge carriers for flow batteries.[24-26] The area cost factors, balance of plant, and additional contributions to price are the same as those for the VRFB. Here, we have assumed that a 1.5-V cell voltage and ASR of 0.5 $\Omega \cdot cm^2$ are possible, considering these same values for the VRFB.[27] Both of these values should be considered development targets. The equivalent molecular weight of 150 $g \cdot (mol \cdot e^-)^{-1}$ and cost of the tailored molecules of \$5 kg^{-1} were selected to approach the cost target of \$120 per kW·h.

Nonaqueous Tailored Molecule Flow Batteries (NAqRFB)

Tailored molecules for nonaqueous electrolytes are far from a commercial reality at the time of this publication. The data in this manuscript produce the first quantitative guidance for researchers to consider in their exploration. Many published works use molecules with high equivalent molecular weights, a wide range of voltages for the redox events, and low solubility.[25, 28-31] The objective of the values used for NAqRFB molecules here is to provide clear goals that are required to reach cost-effective energy storage targets. Some promising molecules have been identified, but an archetype redox couple is not yet established. The values used in this analysis are justified in the main text and above in system considerations.

Hybrid (Enclosed and Flow) Architectures

Zinc Bromide

The Zn/Br_2 flow batteries use a flowing electrolyte for both the positive and negative electrode. However, the zinc cation is plated onto the negative electrode during charge from $ZnBr_2$ anolyte.[32] The Zn metal anode then oxidizes to release the cations on discharge. The positive electrode reduces Br_2 to $ZnBr_2$. In commercial systems, a complexing agent (e.g., N-ethyl-N-methylpyrrolidiniumbromide (MEP)) is used to ensure a vanishingly low vapor pressure for Br_2 gas.[32] Zn/Br_2 systems commonly employ a nanoporous separator rather than an ion-exchange membrane, and have a relatively low coulombic efficiency of around 90% through a single discharge. The crossover Br_2 molecules reduce on the negative electrode. The use of the MEP or other complexing agent reduces the extent of crossover. Graphite plates are used to withstand corrosion from the bromine containing electrolyte. A porous felt is used for the positive electrode. The electrolyte may contain NH_4Cl as a supporting electrolyte. Installed Zn/Br_2 costs for a 5-h discharge are in the range \$330-560 per kW·h.[1] Larsson estimated an installed cost of \$200 per kW·h for a 1-MW system.[33]

Lithium Polysulfide (LiPS)

The nonaqueous hybrid cell utilizes stainless-steel stamped metal plates for the positive electrode flow field, a nanoporous separator, and a carbon felt electrode. The minimum cost factor per unit area includes a case where no carbon felt electrode is used. Here, we capture the potential of suspension-based electrodes for flow batteries.[34, 35] Therein, low volume factions of carbon black, ~2%, are suspended in the electrolyte with the active material. The dispersed carbon acts as a reaction surface and also a current collector network, obviating the need for a stationary carbon felt electrode.

Lithium cells utilizing sulfur-based positive electrodes are reportedly less likely to suffer from dendritic shorts, perhaps owing to the dissolved polysulfide species that promote corrosion of the lithium metal. They would preferentially react with any poorly passivated, high-surface-area growths that protrude from the electrode. This factor, in combination with the potential improvements from a convection-based system, justifies research efforts to examine the behavior of the lithium electrode in a LiPS hybrid flow cell.

Sensitivity analysis has been performed on limiting charging current that results in dramatically different sized reactors. Figure S3 presents projected future prices for useable energy in LiPS batteries. Despite improving charge acceptance, the lithium metal electrode is currently challenged by a persistent decomposition due to the electrolyte, resulting in irreversible capacity loss. This problem is in large part due to a lack of morphology control of lithium during plating as well as the semi-passive film that provides only modest insulation from the electrolyte (i.e., the solid-electrolyte interphase). Novel approaches to mitigating this life-limiting mechanism are needed to enable a lithium metal electrode with minimal capacity fade during calendar aging and irreversible losses on the order 0.01% per cycle.

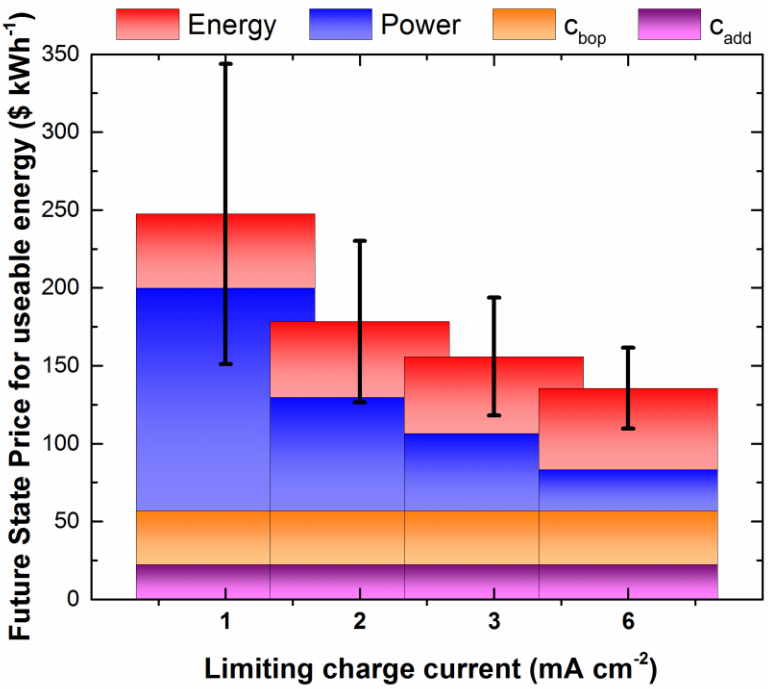

Figure S3. Projected future prices for useable energy in LiPS batteries as a function of the limiting charge current used to determine the reactor power density.

Lithium Nonaqueous Organic Flow

This cell utilizes a lithium metal electrode similar to LiPS, but a high-voltage nonaqueous tailored molecule approach on the positive electrode. There are several molecules that show redox activity above 4.0 V vs. Li.[36-38] However, the solubility of these molecules has not yet been demonstrated to be in line with the goal of >0.8 kg kg^{-1}.

The nonaqueous hybrid cell utilizes stainless-steel stamped metal plates for the positive electrode flow field, a nanoporous separator, and a carbon felt electrode. The minimum cost factor per unit area includes a case where no carbon felt electrode is used. Here, we capture the potential of suspension-based electrodes for flow batteries. Therein, low volume factions of carbon black, ~3%, are suspended in the electrolyte with the active material. The dispersed carbon acts as a reaction surface and also a current collector network, obviating the need for a stationary carbon felt electrode.

Nonaqueous Electrolyte Properties

Table S1 presents literature values for solution conductivities at room temperature in various battery technologies, and Table S2 presents conductivity values for various membrane materials.

Table S1: Solution conductivities at room temperature for various battery technologies

Battery	**Solvent**	**Salt**	**Conductivity (mS cm^{-1})**
Lead Acid[39]	Water	H_2SO_4	136
Nickel Metal Hydride[40]	Water	KOH	400-600
Vanadium Redox[41]	Water	$H_2SO_4/VOSO_4$	150-500
Li/ion[31, 42, 43]	PC	$LiPF_6/LiClO_4/LiBF_4$	3-9
Li/ion[31]	PC	$LiAsF_6$/Li triflate/Li_2NH	2-5
Li/ion[31]	EC/DMC	$LiBF_4/LiPF_6$/ $LiAsF_6$/ $LiClO_4$	8-11

Table S2: Membrane conductivity at room temperature

Membrane Material	**Conductivity (mS cm^{-1})**
Nafion 117 (aqueous)[44]	90
Nafion 117 (strong acid) [44]	50
Nafion 117 (Li^+ non-aqueous)[45, 46]	0.01-10
Solid Electrolyte[47]	0.001-10

Table S3 lists rate constants reported for various redox couples immersed in either water or an organic solvent. The three aqueous couples measured on different electrodes indicate varying degrees of surface sensitivity. According to the table, the vanadium couples, which have successfully been used in flow batteries, yield the lowest reaction rates. This finding appears to suggest that development of couples with acceptably high reaction rates should be possible for both aqueous and nonaqueous electrolytes.

Table S3: Rate constants for various redox couples

Redox couple	**Solvent**	**Electrode**	**Rate constant (cm/s)**
Fe^{3+}/Fe^{2+} [48]	Water	Au(poly)	2.2×10^{-5}
Fe^{3+}/Fe^{2+} [48]	Water	Au(111)	1.2×10^{-5}
Cr^{3+}/Cr^{2+} [48]	Water	Hg	2×10^{-4}
VO_2^{+}/VO^{2+} [48]	Water	Graphite	3.0×10^{-7}
VO_2^{+}/VO^{2+} [48]	Water	Carbon	$1\text{-}3\times10^{-6}$
V^{3+}/V^{2+} [48]	Water	Hg	4×10^{-3}
Ce^{4+}/Ce^{3+} [48]	Water	Pt	1.6×10^{-3}
Br_2/Br^{-} [48]	Water	Pt(poly)	1.7×10^{-2}
Br_2/Br^{-} [48]	Water	Vitreous carbon	5.8×10^{-4}
Ferrocene [49]	EC:EMC	Glassy Carbon	1.4×10^{-3}
TEMPO [50]	Acetonitrile	Pt	2.9×10^{-1}
2,5-di-tert-butyl-1,4-bis(2-methoxyethoxy)benzene (DBBB) [51]	PC	Glassy Carbon	$10^{-4}\text{-}10^{-3}$
V(acac)[9]	Acetonitrile	Glassy Carbon	1.3×10^{-4}
V(acac)[9]	Acetonitrile	Pt	3.9×10^{-4}
V(acac)[9]	Acetonitrile	Gold	8.7×10^{-4}
Li-Polysulfide[51]	TEGDME	Glassy Carbon	3.4×10^{-4}
AQDS[23]	Acetonitrile	Glassy Carbon	7.2×10^{-3}

Pumping work constitutes an important parasitic loss in flow batteries. Laminar flow is encountered in the electrochemical reactor, which leads to pressure losses that are proportional to viscosity. Table S4 shows viscosities for a selection of aqueous and nonaqueous solutions.

Table S4: Viscosities of various battery systems

System	**Solvent**	**Salt**	**Viscosity (cP)**
Lead-acid battery [20]	Water	H_2SO_4	0.5-3
Nickel metal hydride battery [52, 53]	Water	NaOH	1.0-1.7
Vanadium redox battery [41]	Water	$H_2SO_4/VOSO_4$	1-10
Li/ion battery [43, 54]	EC	$LiClO_4$	7.91
Li/ion battery [43, 54, 55]	PC	$LiClO_4$/ $LiBF_4$/ $LiPF_6$	3-8

Flow batteries typically have better mass-transport characteristics than enclosed batteries because of forced flow through the electrodes. The frequently cited correlation of Wilson and Geankoplis indicates that the mass-transfer coefficient is proportional to $D^{2/3}$.[27] The data in Table S5 and Figure S4 suggest that the active species in nonaqueous systems tend to have lower diffusion coefficients than the metallic redox couples commonly used in aqueous flow batteries.[51] Increasing the velocity through the electrodes can overcome any decrease in mass-transfer rates at the cost of higher pressure drop.

Table S5: Diffusion coefficients of solvent and redox material

Solvent	**Redox Material**	**Diffusion Coefficient x10^6 (cm^2/s)**
Water [52]	Br^-	20.8
Water [52]	Zn^{2+}	7.03
Water [52]	Fe^{3+}	6.04
Water [52]	Fe^{2+}	7.19
Water [52]	Cr^{3+}	5.95
Water [52]	Ce^{3+}	6.20
PC[51]	DBBB (ANL RS2)	1
DMC[51]	DBBB (ANL RS2)	1
1:1 EC:EMC[51]	ferrocene	2.4

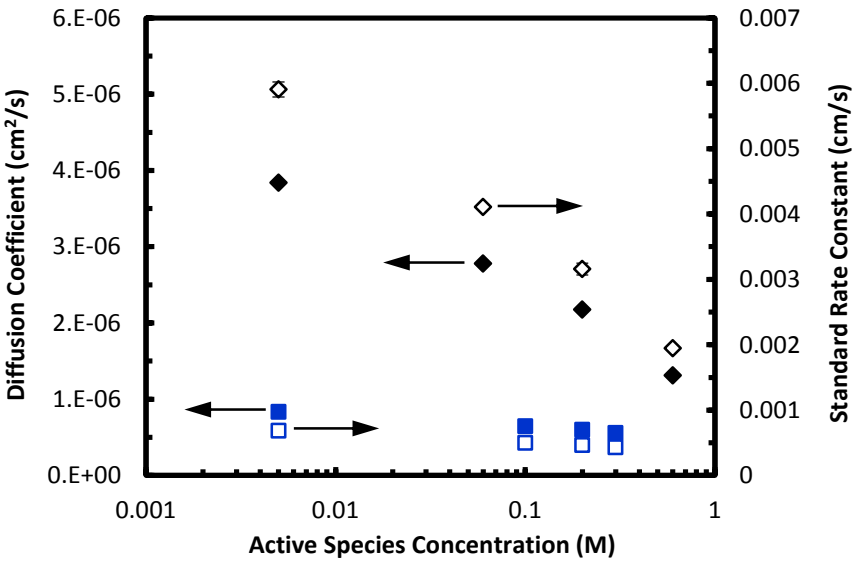

Figure S4: Diffusion coefficient and rate constant of 2,5-di-tert-butyl-1,4-bis(2-methoxyethoxy)benzene (DBBB) measured as a function of concentration. The measured properties decrease marginally with orders of magnitude increase in the concentration of active specie. Measurements completed in 0.9 M LiTFSI in DME (black diamonds) or 0.6 M LiTFSI in PC (blue squares)

The solubility of active species is a critical parameter to offset the higher cost of the nonaqueous electrolytes. In addition to solutions, suspensions of nanoparticles have also been suggested as alternative approach to reach high redox center concentrations in solution.

Table S6: Solubility of active material in solution on the basis of redox centers

Solvent	**Redox Material**	**Solubility (M)**
Water/H_2SO_4 [56]	$VOSO_4$	1.5
Acetonitrile [23]	$V(acac)_3$	0.6
PC/LiTFSI [51]	DBBB (ANL RS2)	0.3
DME/LiTFSI [51]	DBBB (ANL RS2)	0.9
PC [25]	Quinoxaline	~7
TEGDME [35]	Lithium polysulfides (LiPS)	1 – 1.25
TEGDME [35]	Precipitated lithium sulfide	5
EC: EMC / $LiPF_6$ [34]	$Li_4Ti_5O_{12}$ (semi-solid slurry)	2.5
EC:DMC / $LiPF_6$ [34]	$LiCoO_2$ (semi-solid slurry)	11.5
Water/H_2SO_4 [24]	AQDS	> 1

Power density comparison of nonaqueous to aqueous flow batteries

Assuming a 3 V couple for nonaqueous and a 1.5 V couple for aqueous, we can project relative power densities for the ASR presented in the main text. For slower rate constants, the lower electrolyte conductivity of nonaqueous systems is less important. Higher power densities may be achievable by operating at modestly elevated temperatures.

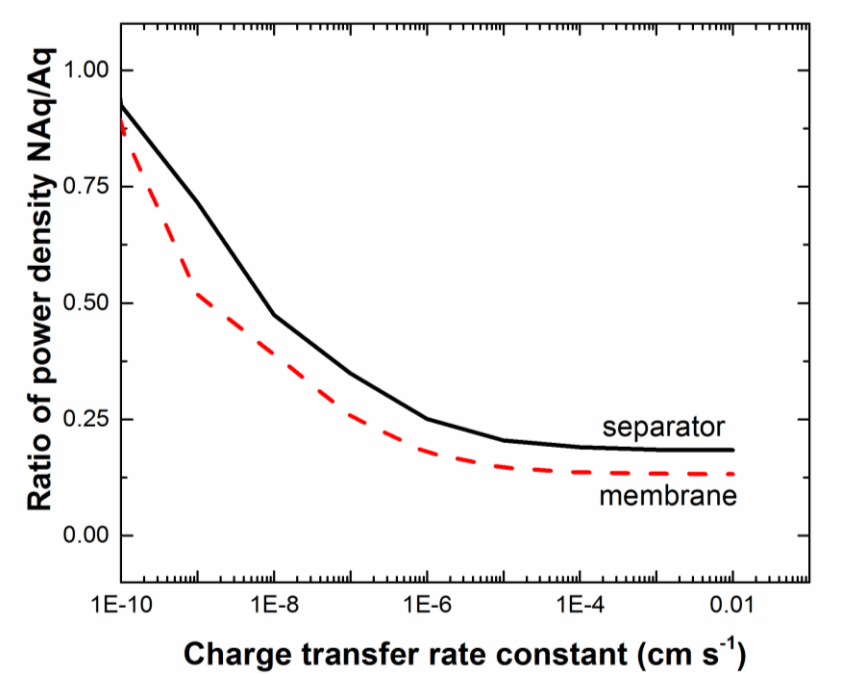

Figure S5: Relative power density of a 3 V nonaqueous flow battery to a 1.5 V aqueous flow battery as a function of charge transfer rate constant.

References:

1. A. A. Akhil, G. Huff, A. B. Currier, B. C. Kaun, D. M. Rastler, S. B. Chen, A. L. Cotter, D. T. Bradshaw and W. D. Gauntlett, *DOE/EPRI 2013 Electricity Storage Handbook in Collaboration with NRECA*, Sandia National Laboratories, Albuquerque, New Mexico 87185 and Livermore, California 94550 2013.
2. V. Viswanathan, A. Crawford, D. Stephenson, S. Kim, W. Wang, B. Li, G. Coffey, E. Thomsen, G. Graff, P. Balducci, M. Kintner-Meyer and V. Sprenkle, *Journal of Power Sources*, 2014, 247, 1040-1051.
3. D. Rastler, *Market Driven Distributed Energy Storage System Requirements for Load Management Applications*, Electric Power Research Institute, Palo Alto, CA, 2007.
4. A. J. Salkind, R. O. Hammel, A. G. Cannone and F. A. Trumbore, in *Handbook of Batteries*, eds. D. Linden and T. B. Reddy, McGraw-Hill, New York, 3rd edn., 1995, ch. 24, pp. 24.21-24.46.
5. P. T. Moseley and J. Garche, *Electrochemical Energy Storage for Renewable Sources and Grid Balancing*, Elsevier Science, 2014.
6. P. Nelson, K. Gallagher, I. Bloom and D. Dees, *Modeling the Performance and Cost of Lithium-Ion Batteries for Electric Vehicles*, Chemical Sciences and Engineering Division, Argonne National Laboratory, ANL-11/32, Argonne, IL USA, 2011.

7. T. E. Lipman, *The Cost of Manufacturing Electric Vehicle Batteries: Report for the California Air Resources Board*, Institute of Transportation Studies, Davis, CA, 1999.
8. P. A. Nelson, K. G. Gallagher and I. Bloom, *BatPaC (Battery Performance and Cost) Software* http://www.cse.anl.gov/BatPaC/, 2012.
9. A. A. Shinkle, A. E. S. Sleightholme, L. T. Thompson and C. W. Monroe, *Journal of Applied Electrochemistry*, 2011, 41, 1191-1199.
10. B. D. James, J. A. Kalinoski and K. N. Baum, *Mass Production Cost Estimation of Direct H2 PEM Fuel Cell Systems for Transportation Applications: 2010 Update*, Directed Technologies, Inc, Arlington, VA, 2010.
11. B. D. James and A. B. Spisak, *Mass Production Cost Estimation of Direct H2 PEM Fuel Cell Systems for Transportation Applications: 2012 Update*, Strategic Analysis Inc, Arlington, VA, 2012.
12. C. Pillot, "The worldwide battery market 2011-2025", Batteries 2012, Nice, France.
13. K. G. Gallagher, S. Goebel, T. Greszler, M. Mathias, W. Oelerich, D. Eroglu and V. Srinivasan, *Energy & Environmental Science*, 2014, 7, 1555-1563.
14. Gigafactory, http://www.teslamotors.com/sites/default/files/blog_attachments/gigafactory.pdf, Accessed June 26, 2014, 2014.
15. R. M. Cuenca, L. L. Gaines and A. D. Vyas, *Evaluation of Electric Vehicle Production and Operating Costs*, Argonne National Laboratory, Lemont, IL, 1999.
16. M. Anderman, F. R. Kalhammer and D. MacArthur, *Advanced Batteries for Electric Vehicles: An Assessment of Performance, Cost, and Availability*, The Year 2000 Battery Technology Advisory Panel prepared for the California Air Resources Board, Sacramento, CA 2000.
17. V. Srinivasan, G. Q. Wang and C. Y. Wang, *Journal of the Electrochemical Society*, 2003, 150, A316-A325.
18. P. T. Moseley, R. F. Nelson and A. F. Hollenkamp, *Journal of Power Sources*, 2006, 157, 3-10.
19. D. A. J. Rand and P. T. Moseley, in *Electrochemical Energy Storage for Renewable Sources and Grid Balancing*, eds. P. T. Moseley and J. Garche, Newnes, Oxford, 2014, ch. 13, p. 360.
20. H. Bode, *Lead-Acid Batteries*, John Wiley & Sons, New York, 1977.
21. G. Yonglang, *Journal of the Electrochemical Society*, 2005, 152, A1136-1141.
22. H. Zheng, J. Li, X. Song, G. Liu and V. S. Battaglia, *Electrochimica Acta*, 2012, 71, 258-265.
23. A. A. Shinkle, A. E. S. Sleightholme, L. D. Griffith, L. T. Thompson and C. W. Monroe, *Journal of Power Sources*, 2012, 206, 490-496.
24. B. Huskinson, M. P. Marshak, C. Suh, S. Er, M. R. Gerhardt, C. J. Galvin, X. Chen, A. Aspuru-Guzik, R. G. Gordon and M. J. Aziz, *Nature*, 2014, 505, 195-+.
25. F. R. Brushett, J. T. Vaughey and A. N. Jansen, *Advanced Energy Materials*, 2012, 2, 1390-1396.
26. D. Amadeo et al, Electrochemical Energy Storage Systems and Methods Featuring large Negative Half-Cell Potentials , WO 2014/019605 A1, 2014.
27. R. M. Darling and M. L. Perry, *Journal of The Electrochemical Society*, 2014, 161, A1-A7.
28. P. J. Cappillino, H. D. Pratt, III, N. S. Hudak, N. C. Tomson, T. M. Anderson and M. R. Anstey, *Advanced Energy Materials*, 2014, 4.

29. L. Qinghua, A. A. Shinkle, L. Yongdan, C. W. Monroe, L. T. Thompson and A. E. S. Sleightholme, *Electrochemistry Communications*, 2010, 12, 1634-1637.
30. W. Wang, W. Xu, L. Cosimbescu, D. Choi, L. Li and Z. Yang, *Chemical Communications*, 2012, 48, 6669-6671.
31. K. Xu, *Chemical Reviews*, 2004, 104, 4303-4417.
32. P. c. Butler, P. A. Eidler, P. G. Grimes, S. E. Klassen and R. C. MIles, in *Handbook of Batteries*, eds. D. Linden and T. B. Reddy, McGraw-Hill, New York, 3rd edn., 1995, ch. 39, pp. 39.31-39.22.
33. A. Larsson, Massachusetts Institute of Technology, 2009.
34. M. Duduta, B. Ho, V. C. Wood, P. Limthongkul, V. E. Brunini, W. C. Carter and Y.-M. Chiang, *Advanced Energy Materials*, 2011, 1, 511-516.
35. F. Y. Fan, W. H. Woodford, Z. Li, N. Baram, K. C. Smith, A. Helal, G. H. McKinley, W. C. Carter and Y.-M. Chiang, *Nano Letters*, 2014, 14, 2210-2218.
36. W. Kempton and J. Tomic, *Journal of Power Sources*, 2005, 144, 280-294.
37. U. Eberle and R. von Helmolt, *Energy & Environmental Science*, 2010, 3, 689-699.
38. M. Contestabile, G. J. Offer, R. Slade, F. Jaeger and M. Thoennes, *Energy & Environmental Science*, 2011, 4, 3754-3772.
39. G. Lindbergh, *Electrochimica Acta*, 1997, 42, 1239-1246.
40. N. Sato and K. Yagi, *Jsae Review*, 2000, 21, 205-211.
41. F. Rahman and M. Skyllas-Kazacos, *Journal of Power Sources*, 2009, 189, 1212-1219.
42. M. S. Ding and T. R. Jow, *Journal of the Electrochemical Society*, 2004, 151, A2007-A2015.
43. G. Pistoia, *Journal of the Electrochemical Society*, 1971, 118, 153-158.
44. Y. Sone, P. Ekdunge and D. Simonsson, *Journal of the Electrochemical Society*, 1996, 143, 1254-1259.
45. M. Doyle, M. E. Lewittes, M. G. Roelofs and S. A. Perusich, *Journal of Physical Chemistry B*, 2001, 105, 9387-9394.
46. M. Doyle, M. E. Lewittes, M. G. Roelofs, S. A. Perusich and R. E. Lowrey, *Journal of Membrane Science*, 2001, 184, 257-273.
47. J. W. Fergus, *Journal of Power Sources*, 2010, 195, 4554-4569.
48. A. Z. Weber, M. M. Mench, J. P. Meyers, P. N. Ross, J. T. Gostick and Q. Liu, *Journal of Applied Electrochemistry*, 2011, 41, 1137-1164.
49. C. O. Laoire, E. Plichta, M. Hendrickson, S. Mukerjee and K. M. Abraham, *Electrochimica Acta*, 2009, 54, 6560-6564.
50. F. Kato, A. Kikuchi, T. Okuyama, K. Oyaizu and H. Nishide, *Angewandte Chemie-International Edition*, 2012, 51, 10177-10180.
51. L. Su, E. Carino and F. Brushett, unpublished work.
52. W. M. Haynes, ed., *CRC Handbook of Chemistry and Physics*, CRC Press, Boca Raton, FL, 2011.
53. J. R. Bourne, P. Dellava, O. Dossenbach and T. Post, *Journal of Chemical and Engineering Data*, 1985, 30, 160-163.
54. D. Aurbach, ed., *Nonaqueous Electrochemistry*, CRC Press, 1999.
55. A. Hofmann, M. Schulz and T. Hanemann, *International Journal of Electrochemical Science*, 2013, 8, 10170-10189.
56. G. Oriji, Y. Katayama and T. Miura, *Electrochimica Acta*, 2004, 49, 3091-3095.